Available online at www.sciencedirect.com

SciVerse ScienceDirect

Ceramics International 39 (2013) 5083–5091

CERAMICS INTERNATIONAL

www.elsevier.com/locate/ceramint

A green and facile one-pot synthesis of Ag–ZnO/RGO nanocomposite with effective photocatalytic activity for removal of organic pollutants

Hem Raj Pant[a,b,*], Bishweshwar Pant[b], Han Joo Kim[c], Altangerel Amarjargal[b,d], Chan Hee Park[b,*], Leonard D. Tijing[c], Eun Kyo Kim[b], Cheol Sang Kim[b,c,*]

[a]Department of Engineering Science and Humanities, Institute of Engineering, Pulchowk Campus, Tribhuvan University, Kathmandu, Nepal
[b]Department of Bionanosystem Engineering, Chonbuk National University, Jeonju 561-756, Republic of Korea
[c]Division of Mechanical Design Engineering, Chonbuk National University, Jeonju 561-756, Republic of Korea
[d]Power Engineering School, Mongolian University of Science and Technology, Ulaanbaatar, Mongolia

Received 10 October 2012; received in revised form 22 November 2012; accepted 1 December 2012
Available online 23 December 2012

Abstract

In this study, Ag–ZnO/reduced graphene oxide (Ag–ZnO/RGO) composite was synthesized by a green and facile one-step hydrothermal process. Aqueous suspension containing Ag and ZnO precursors with graphene oxide (GO) sheets was heated at 140 °C for 2 h. The morphology and structure of as-synthesized particles were characterized by field emission scanning electron microscopy (FE-SEM), transmission electron microscopy (TEM), X-ray diffraction (XRD), Raman spectroscopy, and Photoluminescence (PL) spectroscopy which revealed the formation of composite of metal, metal oxide and RGO. It was observed that the presence of Ag precursor and GO sheets in the hydrothermal solution could sufficiently decrease the size of ZnO flowers. The hybrid nanostructure, with unique morphology, obtained from this convenient method (low temperature, less time, and less number of reagents) was found to have good photocatalytic and antibacterial activity. The perfect recovery of catalyst after reaction and its unchanged efficiency for cyclic use showed that it will be an economically and environmentally friendly photocatalyst.

Keywords: B. Nanocomposites; Hydrothermal; Photocatalyst; Ag–ZnO/RGO

1. Introduction

The application of oxidation process in the development of water treatment gave birth to an improvement of the catalytic degradation of microorganism and toxic dyes present in water. The synthesis of semiconductor photocatalyst (TiO_2, ZnO) in extremely small size (< 50 nm) to provide sufficient surface area for photoreaction and their heterogeneous photocatalyst to prevent the electron–hole (e–h) recombination process for accelerating catalytic reaction are potent in this field [1–8]. Even though the decreasing of particle size is one effective way to increase the surface area of photocatalyst, the agglomeration of such extremely nano-sized particles and difficulty of their recovery from the reaction system after photocatalysis hinders their application in this field. As the recovery of NPs from the reaction system is very difficult, it limits their application environmentally (secondary pollution) and economically (loss of catalyst) [9–11]. It may bring about a breakthrough when these semiconductor NPs can be assembled into about micro-sized particles, which will possess the unique properties of NPs and the easiness of separation and recovery for practical photocatalytic application. Therefore, the formation of flower-shaped ZnO particles (flower provides high surface area) doped with those materials which can assist e–h separation and recovery of photocatalyst from the

*Corresponding authors at: Department of Bionanosystem Engineering, Chonbuk National University, Jeonju 561-756, Republic of Korea. Tel.: +82 63 2704284; fax: +82 63 2702460.
E-mail addresses: hempant@jbnu.ac.kr, hempant2002@yahoo.com (H. Raj Pant), biochan@nate.com (C. Hee Park), chskim@jbnu.ac.kr (C. Sang Kim).

0272-8842/$ - see front matter © 2012 Elsevier Ltd and Techna Group S.r.l. All rights reserved.
http://dx.doi.org/10.1016/j.ceramint.2012.12.003

reaction system after photocatalysis becomes a potential candidate in this field [4,9,12,13].

Graphene is an atomically thin layer of sp2-hybridized carbon atoms arranged in a honeycomb structure which has sufficient surface area and high transparency [14–16]. The good dispersion of graphene oxide (GO) in different solvents and its interaction with other functionalities (of different materials) can offer the formation of nanocomposite with variety of materials. Furthermore, GO sheets can be easily reduced using hydrothermal treatment [17]. Therefore, a simple and effective strategy of simultaneous growth of Ag and ZnO NPs, and reduction of graphene oxide was developed to synthesis Ag NPs doped flower-shaped ZnO nanoparticles on the surface of reduced graphene sheets using one-pot hydrothermal process. Simultaneous reduction of GO sheets and crystal growth of metal and metal oxide NPs can provide a effectively bonded composite on the surface of RGO sheets. Different metals and metal oxides have been used to deposit on the graphene sheets and the resultant composite exhibits superior photocatalytic and other properties [18–21]. Therefore, deposition of Ag doped ZnO flowers on graphene sheets is an efficient way to construct composite photocatalyst to improve the properties of ZnO by utilizing the unique properties of graphene and silver. The fix attachment of NPs on the surface of high aspect ratio graphene sheets not only prevents from the loss of photocatalyst during recovery but also assists e–h separation during photocatalytic process.

2. Experimental

2.1. Materials

Synthetic graphite from Aldrich (average particle diameter < 20 μm) was used for GO preparation. Potassium permanganate, hydrogen peroxide, sulfuric acid, zinc nitrate hexahydrate, bis-hexamethylene triamine, silver nitrate, reactive black 5 (RB5), and methylene blue (MB) (all AR grade) were used without any further purification.

2.2. Preparation of graphene oxide

Graphene oxide nanosheets were synthesized using a modified Hummer's method [22,23] where 125 ml of concentrated sulfuric acid was taken into 500 ml three necked round bottom flask filled with graphite powder (5 g) followed by the addition of solid potassium permanganate (17.5 g) slowly at 0 °C (ice bath). This mixture was agitated by Teflon coated stirrer for 3 h at 35 °C and then diluted by adding sufficient amount of distilled water at 0 °C (ice bath). H_2O_2 (30 vol% in water) was added until the bubbling of the gas was completed. The product, obtained in this way, was made free from acid by centrifuging and washing several times with deionized water and subsequently dried under vacuum at 70 °C for two days. The desired brown powder of graphite oxide was obtained.

2.3. Preparation of photocatalysts

\As-synthesized GO (10 mg) was dissolved in 10 mL of distilled water and ultrasonically exfoliated in a bath sonicator for 30 min. Similarly, solutions containing 0.5 g of bis-hexamethylene triamine in 30 ml water, 0.75 g zinc nitrate hexahydrate in 40 ml water, and 10 mg $AgNO_3$ in 10 ml water were prepared. Zinc nitrate and bis-hexamethylene triamine solutions were mixed with vigorous stirring for further 30 min. In this slurry, GO, $AgNO_3$ and 10 ml ethanol was added. The autoclave with Teflon crucible (containing solution) was kept at 140 °C for 2 h as reported in authors previous work [4]. Similarly, pristine ZnO flowers and Ag–ZnO composite particles were prepared without GO and $AgNO_3$, and GO, respectively. The obtained product after cooling was filtered off, washed several times with distilled water and alcohol, and dried at 130 °C for 12 h before analysis.

2.4. Characterization

The morphology of the as-prepared pristine and composite ZnO particles was examined by using FE-SEM (Hitachi S-7400, Japan). TEM images and line EDX were observed using transmission electron microscopy (JEM-2200, JEOL, Japan). The structure and phase composition of the resulted samples were obtained with a Rigaku X-ray diffractometer (XRD, Rigaku, Japan) with Cu Kα ($\lambda =$ 1.540 Å) radiation over Bragg angles ranging from 0 to 80°. Raman spectra were acquired using FT-Raman spectroscopy (RFS-100 S, Bruker, Germany). Room temperature photoluminescence (PL) spectrum was recorded by Perkin Elmer Instruments (LS-55).

2.5. Photocatalytic activity

The photocatalytic activity was evaluated by observing the degradation of the solutions of MB and RB5. The process was carried out in a 100 ml beaker which was equipped with the tip of a light-guide (5 mm in diameter) of mercury-vapor lamp (OmniCure, EXFO). The UV light of very low intensity (2.2 W/cm^2, 20%) was used in this experiment. The distance between solution and tip of light-guide was 5 cm. In each case, 30 ml of dye solution (10 ppm) and 20 mg catalyst were mixed to make suspension by stirring for 30 min in dark before UV irradiation. Prior to irradiation, different photocatalysts and dye solutions were magnetically stirred for 10 min under dark conditions to establish an adsorption/desorption equilibrium between dyes and photocatalyst surface. At specific time intervals, 1 ml of the sample was withdrawn from the system and centrifuged to separate the residual catalyst, and then the absorbance intensity was measured at the corresponding wavelength. The composite photocatalyst without UV irradiation (in dark) was taken as control. For cycling use experiments, Ag–ZnO–RGO NPs were separated from suspended solution by repeated centrifuging and washing process.

2.6. Antibacterial property

Bacterial inactivation test was carried out using *Escherichia coli* (*E. coli*) as the model organism. One colony of *E. coli* was taken out from the original stock in an agar plate and was cultured lysogeny broth (LB) medium at 500 μl. This bacterial solution was incubated at 35 ± 0.1 °C. The working suspensions were prepared by adding 200 μl of inoculated LB medium to a 50 ml sterilized distilled water in a beaker and antibacterial experiment was carried out in a sterilized 100 ml glass beaker containing *E. coli* suspension (50 ml) and 0.4 g/l of different photocatalysts with magnetic stirring. The initial bacterial concentration was maintained at 107 CFU/ml and the tests were performed at room temperature for 120 min. The UV light intensity was maintained at 2.2 W/cm^2 (only 20%) using a mercury vapor lamp (OmniCure, EXFO) in which beaker was equipped with the tip of a light-guide (5 mm in diameter) of mercury vapor lamp on the distance of 5 cm. At given time intervals, 1 ml suspension was collected and diluted appropriately by serial dilution in distilled water. To count the bacterial concentration, ready-to-use petrifilm (3 M Petrifilm, USA) and prepared agar plates were used. After incubation for 48 h, the number of bacteria was manually counted using a colony counter. Furthermore, zone inhibition method was also carried out to measure the antibacterial activity of different photocatalyst on *E. coli*. Using a spread plate method, nutrient agar plates were incubated with 1 ml of bacterial suspension containing around 106 colony forming units (CFU)/ml. The photocatalysts were gently placed on the inoculated plates, and were then incubated at 37 °C for 24 h. Zones of inhibition were determined by measuring the clear area formed around each photocatalyst.

3. Results and discussion

3.1. Characterizations of photocatalysts

FE-SEM images of ZnO, Ag–ZnO, and Ag–ZnO/RGO photocatalysts are shown in Fig. 1. It shows that pristine ZnO particles are micro sized flower-like structure and their size decreases when Ag precursor and GO sheets are added into the hydrothermal solution (Fig. 1b and c). Well dispersed GO sheets throughout the solution and dissolved $AgNO_3$ could decrease the amount of ZnO precursor per unit volume and consequently decrease the size of ZnO flowers. It is clear from Fig. 1b that $AgNO_3$ containing solution not only decreases the size of ZnO flowers but also deposits Ag NPs on the surface of flowers (inset of Fig. 1b). The addition of GO sheets could further decreases the size of flowers and ZnO particles were well attached on the surface of crumbled structure reduced graphene sheets (shown by arrow in Fig. 1c). The simultaneous formation of metal and metal oxide crystal with reduction of GO by this one-step process, chemically bonded ZnO/RGO is believed to be formed through the interactions between Zn and oxygen-containing functional groups in GO followed by removal of these groups during the hydrothermal treatment [17]. Furthermore, deposited Ag NPs were properly attached on the surface of ZnO flowers and RGO sheets (Fig. 2a). In GO containing solution, numerous separate GO sheets were formed and their thinner sheets with highly exposed oxygen functional groups could provide sufficient anchoring sites for the crystal growth of large numbers of small sized ZnO flowers and Ag NPs. The low magnification TEM images (Fig. 2a) revealed a unique flower-shaped morphology of ZnO particles on the surface of RGO sheets. ZnO flowers as well as RGO sheets were well decorated with Ag NPs (inset of Fig. 2a) which was further supported by TEM-EDX (Fig. 1b). The sizes of Ag NPs were smaller on RGO sheets compared to those which were deposited on ZnO flowers. This result revealed that numerous functionalities present on high aspect ratio GO sheets could act as nucleation sites for deposition of Ag NPs and large numbers of small sized Ag NPs were more favorable on GO sheets compared to the surface of ZnO particles. The formation of metal (Ag) and metal oxide (ZnO) composite by simultaneous nucleation of both particles was observed by line TEM-EDX, shown in Fig. 2c. Here, Ag and ZnO were found along the selected line and revealed the formation of composite in nano structure.

The crystalline structure of as-prepared pristine and Ag–ZnO/RGO composite with the corresponding 2θ values and crystal planes are presented in Fig. 3. All the diffraction peaks for ZnO can be indexed to wurtzite structure (JCPDS card no. 80-0075) for both pristine and composite samples which are similar to the author's previous report [4]. The extra peaks on composite particles compared to

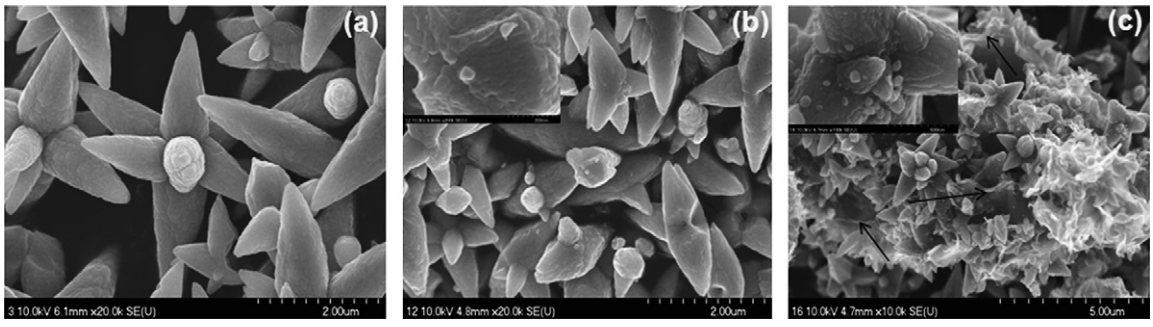

Fig. 1. FE-SEM images of (a) pristine ZnO micro-flowers and (b) Ag–ZnO, and (c) Ag–ZnO/RGO composite (insets of (b) and (c) are their corresponding higher magnification FE-SEM).

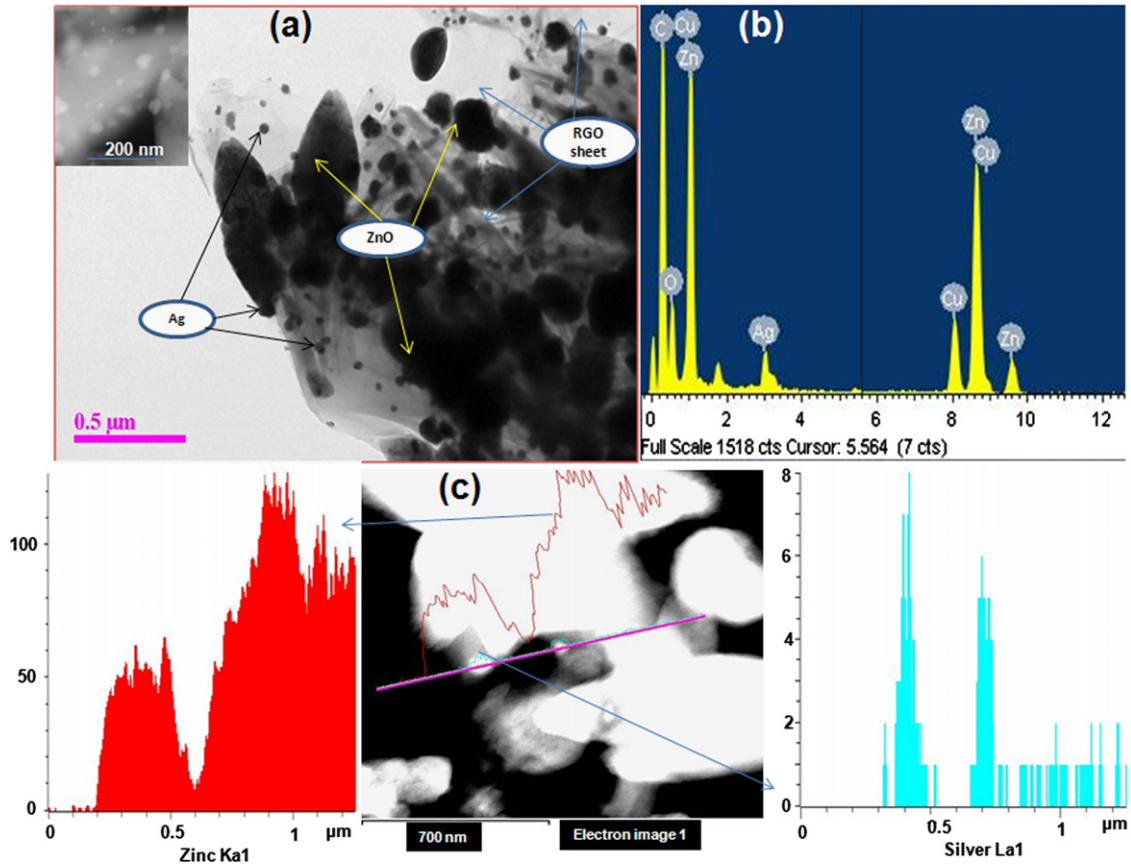

Fig. 2. (a) TEM image, (b) TEM-EDX, and (c) line TEM-EDX of of Ag–ZnO/RGO composite (inset of (a) is TEM image showing Ag NPs on ZnO flowers).

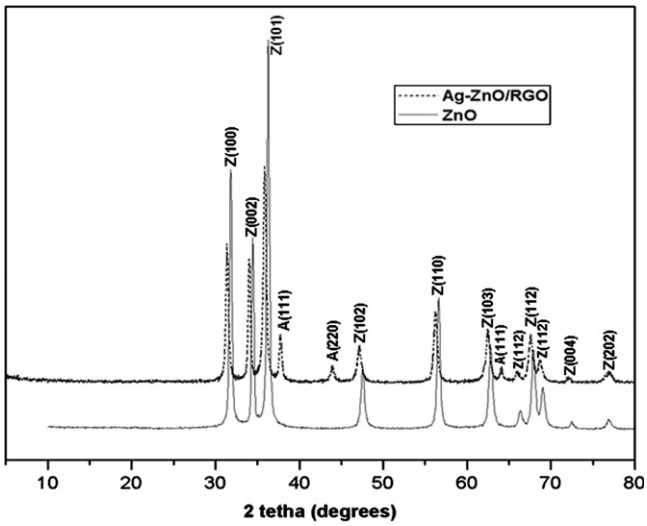

Fig. 3. XRD patterns of as-prepared ZnO and Ag–ZnO/RGO composite (A for Ag and Z for ZnO).

pristine ZnO flowers at 2θ values of 37.8, 44, and 64° corresponding to the crystal planes (111), (200), and (220), respectively, indicated the presence of Ag metal (JCPDS card no. 04-0783). In Ag–ZnO/RGO composite, no diffraction peaks related to carbon could be detected, implying that the reduced graphene oxide sheets were completely exfoliated due to the loading of ZnO flowers and Ag NPs on their surfaces. Furthermore, the diffraction peaks of the ZnO in Ag–ZnO/RGO were shifted to small degree compared with the peaks of pure ZnO which indicated that the lattice constants of ZnO had changed because of the presence of the carbonaceous material [12]. This result indicated that there was an effective interaction between RGO and ZnO particles.

The reduction of GO during hydrothermal treatment was confirmed by Raman spectra. Fig. 4 shows the Raman spectra of as-synthesized ZnO, GO, Ag–ZnO, and Ag–ZnO/RGO. It is well known that GO exhibits two characteristic main peaks for D band at 1335 cm^{-1} and G bands at 1582 cm^{-1}. The G band is attributed to all sp2 carbon forms and provides information on the in-plane vibration of sp2 bonded carbon atoms while the D band suggests the presence of sp3 defects [24]. It was found that the composite showed relatively higher intensity of D to G band where the intensity ratio of D/G (ID/IG) was increased in RGO composite (after hydrothermal) compared to GO (before hydrothermal) which confirmed the reduction of GO sheets during hydrothermal treatment [25]. The peak at around 435 cm^{-1} in pristine ZnO corresponds to E_2 (high) mode [22] is the characteristic peak of hexagonal wurtzite phase of ZnO [26]. The intensity of this peak was remarkably reduced in composite compared to

pristine ZnO due to the possible interaction between ZnO and RGO. Therefore, Raman spectra not only confirmed the reduction of GO but also supported the formation of wurtzite-type crystal with carbonious ZnO during hydrothermal treatment.

Room temperature photoluminescence (PL) spectra of as-synthesized photocatalysts are shown in Fig. 5. The spectra mainly consist of two emission bands. The first band is the UV near-band-edge (NBE) emission with a wavelength of $\approx$ 395 nm [27]. Sharp NBE emission peak is attributed to the recombination of photogenerated electrons and holes [28]. The decreased in intensity at 390 nm in composite particles indicates that the rate of recombination between photogenerated electrons and holes might be lower, which is beneficial for photocatalytic process. The lowest intensity of this peak in Ag–ZnO/RGO is the indication of its highest photocatalytic efficiency. The PL spectrum also shows a strong intense peak around $\approx$ 575 nm which can be likely attributed interstitial oxygen [28,29]. The weak blue emission peak at 448 nm most likely occurs from the donor level of Zn interstitial to acceptor energy level on Zn valency [30]. The blue-green band around 485 nm is probably caused by radiative transition of electron from shallow donor levels, created by the oxygen vacancy to valence band [31].

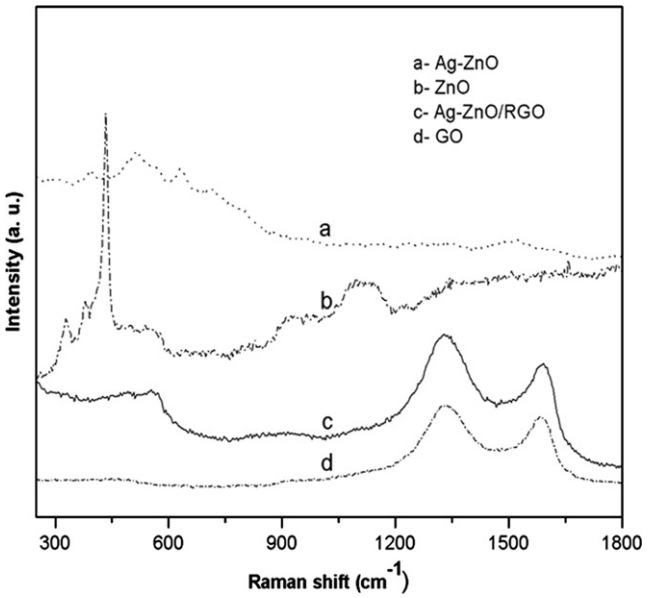

Fig. 4. Raman spectra of different photocatalysts and GO powder.

3.2. Photodegradation of dyes

It is well known that semiconductor particles attached with metals or graphene sheets have been used as an effective photocatalyst for the degradation of organic pollutants in aqueous solution. The photodegradation efficiency can be affected by the size and structure of ZnO particles as well as their manner of attachment on the surface of graphene sheets. Since the flower-shaped ZnO particles decorated with Ag NPs on the surface of RGO sheets exhibit highly open morphologies even though their size is large, they should possess sufficient surface areas and easy to separate from the reaction mixture, and thus become potentially useful as a photocatalyst for degradation of organic pollutants. The photocatalytic activity of the as-synthesized photocatalysts was evaluated by the degradation of MB (cationic dye) and RB5 (anionic dye) under mild UV irradiation (20% intensity). From Figs. 6 and 7, it is clear that the efficiency of ZnO flowers is greatly increased when composite is formed with Ag or Ag/RGO. This outcome may occur because of the unique properties of Ag NPs and RGO sheets provided to ZnO flowers.

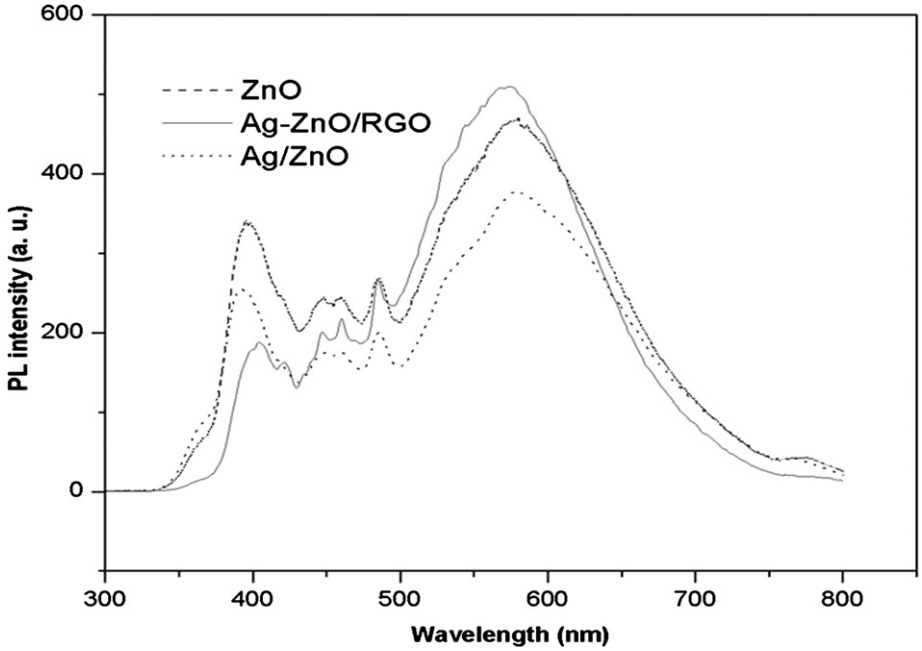

Fig. 5. PL spectra of different photocatalysts.

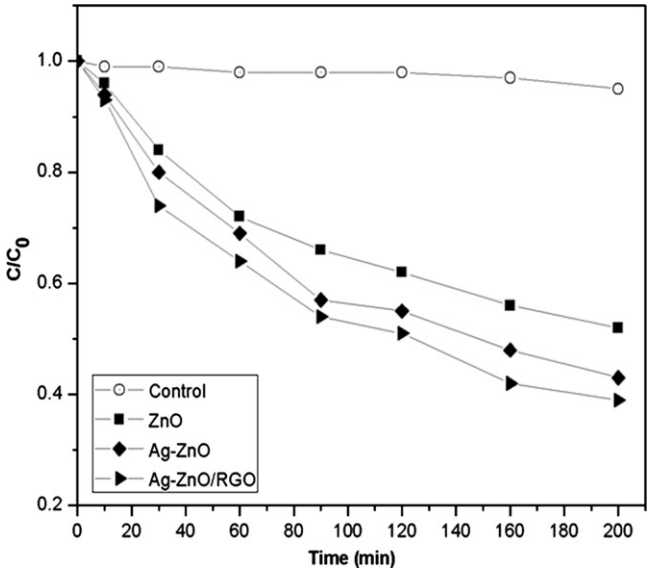

Fig. 6. Comparison of the MB photodegradation in different specimen under UV radiation.

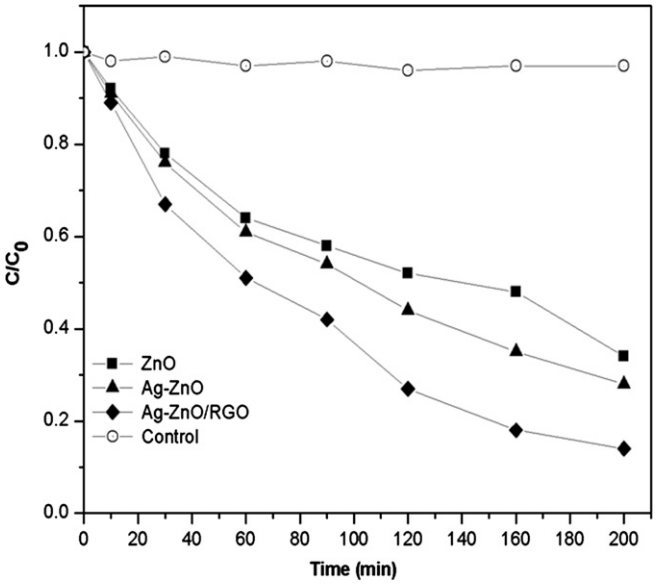

Fig. 7. Comparison of the reactive black 5 photodegradation in different specimen under UV radiation.

Ag NPs deposited on the ZnO flowers as well as RGO sheets attached with ZnO act as electron traps and enhance the e–h separation and the subsequent transfer of trapped electrons to the adsorbed O_2, which acts as an electron acceptor as shown in Fig. 8 [32]. Furthermore, higher chemical activity of the Ag-loaded ZnO can be explained by considering the formation of locally Schottky junctions (by Ag) with high potential gradients established by Schottky barrier than at the ZnO/dye interface. Therefore, efficient charge separation of the light-generated e–h pairs could be achieved [33–35] which was also confirmed from decreased intensity of PL spectra described in Section 3.1. Similarly, the excellent photocatalytic activity of Ag–ZnO/RGO photocatalyst is attributed to these

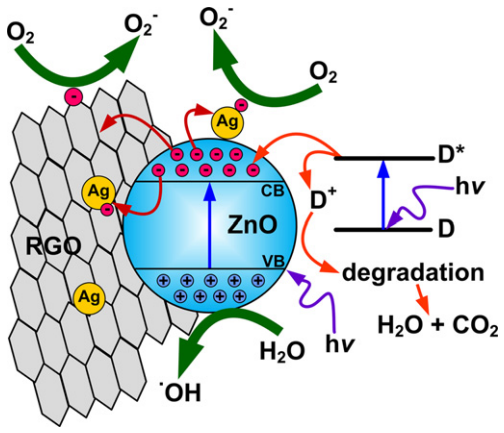

Fig. 8. The schematic diagram of the mechanism of dye degradation over Ag–ZnO/RGO photocatalyst under UV irradiation (D=dye molecules).

three regions: (1) RGO provides a two-dimensional support as well as enough surface area for the deposition of ZnO and Ag NPs. (2) RGO sheets can enhance adsorption ability of the composite. (3) Most important is correlation with the particular electronic properties of the graphene. It is reported that graphene as electron acceptor is a competitive candidate for the electron acceptor material due to its two dimensional π-conjugation structure [36]. It may consider that in Ag–ZnO/RGO composite, the excited electrons of ZnO can quickly transfer from the conduction band of ZnO to the RGO as well as Ag as shown in Fig. 8, and then effectively suppresses the recombination of photo-generated charge carriers, leaving more charge carriers to form highly reactive species (O_2^-, •OH) and promote the degradation of dyes (Fig. 8). Our photoluminescence data (Fig. 5) also supported this mechanism. The low intensity of the peak at 385 nm in composite with compared to the pristine ZnO indicated that the rate of recombination between photogenerated e–h might be lower, which should be beneficial for photocatalytic process [28]. Our photocatalytic results showed that the rate of degradation of reactive black 5 was faster than that of MB. Furthermore, Ag–ZnO/RGO composite not only showed better efficiency than Ag–ZnO but also indicated that the efficiency difference between Ag–ZnO and Ag–ZnO/RGO composite was higher in RB5 degradation compared to the MB degradation (Figs. 6 and 7). This result confirmed that RGO sheets could adsorb anionic dyes (RB5) better than cationic dyes (MB). Ramesha et al. [37] also reported that RGO could adsorb anionic dyes more effectively compared to cationic dyes. Effective adsorption of anionic dye (compared to cationic dye) could promote the dye sensitized mechanism along with the usual ZnO sensitization in Ag–ZnO/RGO photocatalyst as shown in Fig. 8 [38]. Therefore pronounced difference was observed between Ag–ZnO and Ag–ZnO/RGO composite in RB5 degradation compared to MB degradation. The efficiency of composite photocatalyst in recycle use was also evaluated in this work (Fig. 9). It was found that the efficacy of initially used and reused composite photocatalyst up to three cycles was nearly same for the degradation of RB5. The slightly decreased in photocatalytic activity during cyclic use might be

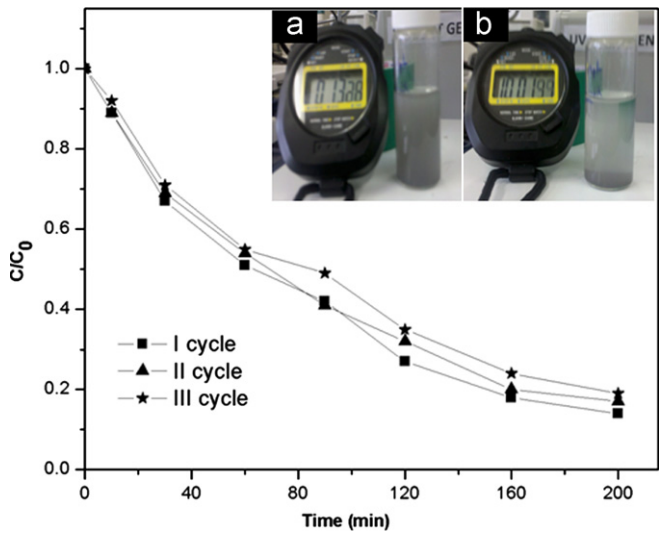

Fig. 9. Catalytic reusability efficiency of Ag–ZnO/RGO nanocomposite up to three-cycles during reactive black 5 degradation (inset is before (a) and after (b) 10 min of sedimentation of 3 h photocatalysed Ag–ZnO/RGO composite).

due to the accumulated organic intermediates on the surface of the catalyst which could affect the adsorption of dyes.

Economically and environmentally friendly photocatalyst should provide easiness of particles separation and their recovery from the reaction system after photocatalysis for practical application. Therefore, we performed a recovery test of as-synthesized photocatalyst from their aqueous suspension. For the separation ability test of photocatalysts, we performed sedimentation process of three hours photodegraded solution (under UV light with continuous stirring) of composite Ag–ZnO/RGO photocatalysts. The inset of Fig. 9 is the photograph of Ag–ZnO/RGO composite after 10 min of sedimentation which shows that the sedimentation of composite photocatalyst is almost completed within 10 min. Therefore, one of the advantages of our as-synthesized photocatalytic particles is that they can be conveniently separated to recycle the catalyst.

3.3. Antibacterial properties

Our concern was not only making a repeatedly useable photocatalyst but also making antibacterial material even in the absence of UV light. Therefore, Ag NPs were simultaneously deposited on the surface of ZnO flowers and RGO sheets. The combined effect of Ag and RGO on the antibacterial efficiency of ZnO flowers was evaluated using mild UV irradiation of bacterial solution at room temperature. Furthermore, their antibacterial capacity without UV light was evaluated by the zone inhibition method. Fig. 10 shows the antibacterial effect of as-prepared photocatalyst under mild (20% intensity) UV radiation. It shows that Ag–ZnO/RGO has the best antimicrobial effect among the synthesized catalysts. The cause of the highest antibacterial capacity of Ag–ZnO/RGO under UV radiation is same as explained in the

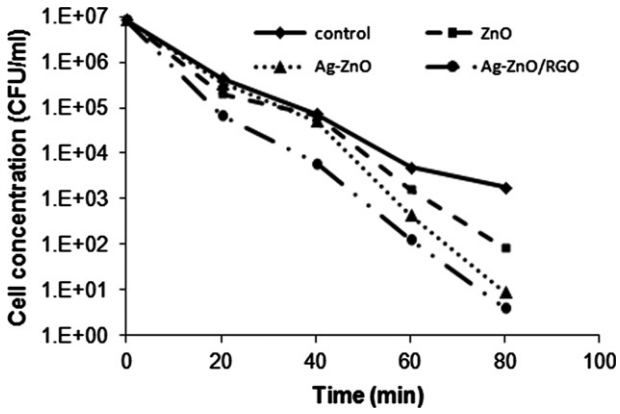

Fig. 10. Antibacterial efficiency of different photocatalysts on gram-negative *E. coli* bacteria under mild UV radiation.

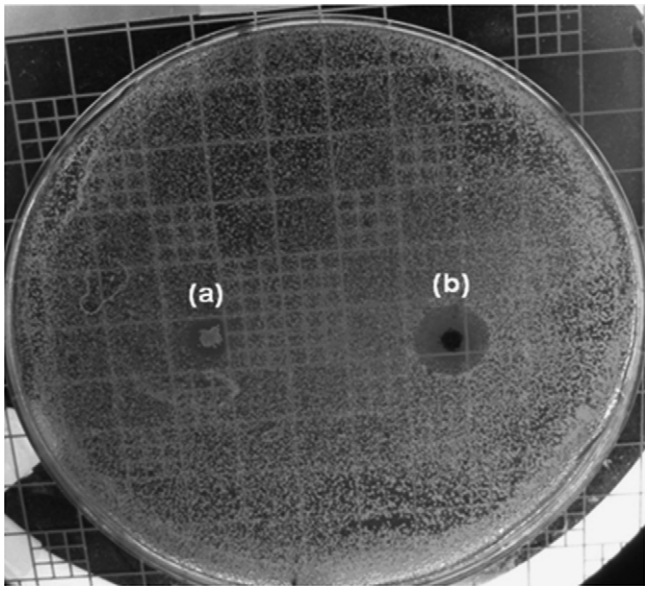

Fig. 11. Zones of inhibition tests for (a) Ag–ZnO and (b) Ag–ZnO/RGO composites towards gram-negative *E. coli* bacteria.

Section 3.2 (Fig. 8). However, far better activity of Ag–ZnO/RGO (Fig. 11b) without UV radiation is attributed to the size and distribution of Ag NPs on the surface of ZnO or ZnO/RGO particles. It is clear from the FE-SEM (inset of Fig. 1b and c) and TEM images (Fig. 2a) that the size of Ag NPs is smaller on the surface of RGO sheets compared to the particles on the surface of ZnO flowers. Furthermore, larger numbers with smaller size of Ag NPs were observed on the Ag–ZnO/RGO composite compared to the Ag/ZnO (Fig. 2a). Increased number of Ag NPs with smaller size could provide more Ag^+ ions around the composite for destruction of bacteria. Therefore, the diameter of the bacterial inhibition zone for Ag–ZnO/RGO showed higher inhibitory efficiency, (i.e., larger clear area around the sample as compared to Ag–ZnO) (Fig. 11). The actual mechanism of killing microorganisms with Ag in absence of UV light is not clear. Some researchers have proposed that Ag has innate antibacterial activity [39]. It is reported that Ag^+ hinders DNA replication

and inhibits the expression of ribosomal proteins and enzymes for ATP hydrolysis [40]. It is also believed that Ag nanoparticles display the same mechanism as Ag^+ and create a redox imbalance, which causes extensive bacterial death. Furthermore, the antibacterial activity of Ag NPs on the surface of the ZnO NPs or RGO sheets may be due to the plasmon resonance of the Ag NPs. Here, photoexcited electrons may transfer from the surface of Ag NPs to the RGO sheets as well as conduction band of ZnO. On the surface of the ZnO NPs, the injected electrons from Ag NPs are trapped by O_2 molecules and the active species such as O_2^-, •OOH, •OH can be generated [41].

4. Conclusions

In summary, we have reported one-pot synthesis of novel composite photocatalyst of metal, metal oxide, and RGO (Ag–ZnO/RGO) using a green and facile hydrothermal technique. Ag–ZnO/RGO composite displayed excellent photocatalytic performance which was attributed to a thin two-dimensional sheet support that provided a good electron acceptor favoring the transfer of photogenerated electrons from the conduction band of ZnO to RGO sheets and Ag NPs. Results showed that as-synthesized Ag–ZnO/RGO photocatalyst had better affinity towards anionic dyes compared to the cationic dyes. Furthermore, Ag decorated semiconductor particles attached on the high surface area RGO sheets not only provided the easiness of particles recovery from reaction system after reaction but also showed the excellent antibacterial efficiency even in the absence of UV radiation. The presented composite photocatalyst synthesis protocol is a simple, fast, efficient, less toxic, and low-cost to produce unique photocatalyst.

Acknowledgments

Hem Raj Pant kindly acknowledges the grant from "CBNU Grant Fellow Project-2012", Chonbuk National University. We also acknowledge the research funds supported by the Korean Ministry of Education, Science and Technology (MIST) through the National Research Foundation (NRF) (Project no. 2012-013423 and 2012-0001611). We would also like to thank Mr. Lee Young-Boo and Mr. T. S. Bae, KBSI, Jeonju branch for TEM and FE-SEM images, respectively.

References

[1] A.I. Hochbaum, P.D. Yang, Semiconductor nanowires for energy conversion, Chemical Reviews 110 (2010) 527–546.
[2] S. Music, D. Dragcevic, S. Popovic, Influence of synthesis route on the formation of ZnO particles and their morphologies, Journal of Alloys and Compounds 429 (2007) 242–249.
[3] K.R. Raghupathi, R.T. Koodali, A.C. Manna, Size-dependent bacterial growth inhibition and mechanism of antibacterial activity of zinc oxide nanoparticles, Langmuir 27 (2011) 4020–4028.
[4] H.R. Pant, C.H. Park, B. Pant, L.D. Tijing, H.Y. Kim, C.S. Kim, Synthesis, characterization, and photocatalytic properties of ZnO nano-flower containing TiO_2 NPs, Ceramics International 38 (2012) 2943–2950.
[5] Z. Li, Y. Luan, Q. Wang, G. Zhuang, Y. Qi, Y. Wang, C. Wang, ZnO nanostructure construction on zinc foil: the concept from an ionic liquid precursor aqueous solution, Chemical Communications (2009) 6273–6275.
[6] L.E. Greene, M. Law, J. Goldberger, F. Kim, J.C. Johnson, Y.F. Zhang, R.J. Saykally, P.D. Yang, Low-temperature wafer-scale production of ZnO nanowire arrays, Angewandte Chemie International Edition 42 (2003) 3031–3034.
[7] L.E. Greene, M. Law, D.H. Tan, M. Montano, J. Goldberger, G. Somorjai, P. Yang, General route to vertical ZnO nanowire arrays using textured ZnO seeds, Nano Letters 5 (2005) 1231–1236.
[8] A.K. Geim, K.S. Novoselov, The rise of graphene, Nature Materials 6 (2007) 183–193.
[9] J. Zhao, Y. yang, Photocatalytic oxidation for indoor air purification: a literature review, Building and Environment 38 (2003) 645–654.
[10] L. Reijenders, Hazard reduction for the application of titania nanoparticles in environmental technology, Journal of Hazardous Materials 152 (2008) 440–445.
[11] H.R. Pant, M.P. Bajgai, Ki Taek Nam, A. Seo, D.R. Pandeya, S.T. Hong, H.Y. Kim, Electrospun nylon-6 spider-net like nanofiber mat containing TiO_2 nanoparticles: a multifunctional nanocomposite textile material, Journal of Hazardous Materials 185 (2011) 124–130.
[12] D. Fu, G. Han, Y. Chang, J. Dong, The synthesis and properties of ZnO–graphene nano hybrid for photodegradation of organic pollutant in water, Materials Chemistry and Physics 132 (2012) 673–681.
[13] H.R. Pant, et al., Antibacterial and photocatalytic properties of Ag/TiO_2/ZnO nano-flowers prepared by facile one-pot hydrothermal process, Ceramics International (2012).
[14] M. Ishigami, J.H. Chen, W.G. Cullen, M.S. Fuhrer, E.D. Williams, Atomic structure of graphene on SiO_2, Nano Letters 7 (2007) 1643–1648.
[15] R.R. Nair, P. Blake, A.N. Grigorenko, K.S. Novoselov, T.J. Booth, T. Stauber, N.M.R. Peres, A.K. Geim, Fine structure constant defines visual transparency of graphene, Science 320 (2008) 1308.
[16] M.J. McAllister, J.L. Li, D.H. Adamson, H.C. Schniepp, A.A. Abdala, J. Liu, M. Herrera-Alonso, et al., Single sheet functionalized graphene by oxidation and thermal expansion of graphite, Chemistry of Materials 19 (2007) 4396–4404.
[17] H. Zhang, X. Lv, Y. Li, Y. Wang, J. Li, P25-graphene composite as a high performance photocatalyst, ACS Nano 4 (2010) 380–386.
[18] A. d Lucas, P.B. Garcia, A. Garrido, A. Romero, J.L. Valverde, Catalytic synthesis of carbon nanotubes with different graphene plane alignments using Ni deposited on iron pillared clays, Applied Catalysis A 301 (2006) 123–132.
[19] D. Wang, D. Choi, J. Li, Z. Yang, Z. Nie, R. Kou, et al., Ternary self-assemblyof ordered metal oxide–graphene nanocomposites for electrochemical energy storage, ACS Nano 3 (2009) 907–914.
[20] S.M. Paek, E.J. Yoo, I. Honma, Enhanced cyclic performance and lithium storage capacity of SnO_2/graphene nanoporous electrodes with three-dimensionally delaminated flexible structure, Nano Letters 9 (2009) 72–75.
[21] G. Jiang, Z. Lin, C. Chen, L. Zhu, Q. Chang, N. Wang, W. Wei, H. Tang, TiO_2 nanoparticles assembled on graphene oxide nanosheets with high photocatalytic activity for removal of pollutants, Carbon 49 (2011) 2693–2701.
[22] S. Park, J. An, R.D. Piner, I. Jung, D. Yang, A. Velamakanni, S.T. Nguyen, R.S. Ruoff, Aqueous suspension and characterization of chemically modified graphene sheets, Chemistry of Materials 20 (2009) 6592–6594.
[23] W.S. Hummers, R.E. Offeman, Preparation of graphitic oxide,, Journal of the American Chemical Society 80 (1985) 1339.

[24] D. Yang, A. Velamakanni, G. Bozoklu, S. Park, M. Stoller, R.D. Piner, S. Stankovich, I. Jung, D.A. Field, C.A. Ventrice, R.S. Ruoff, Chemical analysis of graphene oxide films after heat and chemical treatments by X-ray photoelectron and Micro-Raman spectroscopy, Carbon 47 (2009) 145.

[25] I.K. Moon, J. Lee, R.S. Ruoff, H. Lee, Reduced graphene oxide by chemical graphitization, Nature Communications 1 (2010) 1–6.

[26] X.Y. Ye, Y.M. Zhou, Y.Q. Sun, J. Chen, Z.Q. Wang, Preparation and characterization of Ag/ZnO composites via a simple hydrothermal route, Journal of Nanoparticle Research 11 (2009) 1159–1166.

[27] J. Lim, K. Shin, H.W. Kim, C. Lee, Effect of annealing on the photoluminescence characteristics of ZnO thin films grown on the sapphire substrate by atomic layer epitaxy, Materials Science and Engineering B 107 (2004) 301–304.

[28] J. Yang, J. Zheng, H. Zhai, X. Yang, L. Yang, Y. Liu, J. Lang, M. Gao, Oriented growth of ZnO nanostructures on different substrates via a hydrothermal method, Journal of Alloys and Compounds 489 (2010) 51–55.

[29] J.H. Yang, J.H. Zheng, H.J. Zhai, L.L. Yang, Low temperature hydrothermal growth and optical properties of ZnO nanorods, Crystal Research and Technology 44 (2009) 87–91.

[30] X.Q. Wei, B.Y. Man, M. Liu, C.S. Xue, H.Z. Zhuang, C. Yang, Blue luminescent centers and microstructural evaluation by XPS and Raman in ZnO thin films annealed in vacuum, N_2 and O_2, Physica B: Condensed Matter 60 (2007) 145–152.

[31] D. Chu, Y. Zeng, D. Jiang, Hydrothermal synthesis and optical properties of Pb^{2+} doped ZnO nanorods, Materials Letters 60 (2006) 2783–2785.

[32] A.L. Linsebigler, G. Lu, J.T. Yates, Photocatalysis on TiO_2 surfaces: principles, mechanisms, and selected results, Chemical Reviews 95 (1995) 735–758.

[33] C.Y. Wang, C.Y. Liu, X. Zheng, J. Chen, T. Shen, The surface chemistry of hybrid nanometer-sized particles I. Photochemical deposition of gold on ultrafine TiO_2 particles, Colliods and Surfaces A 131 (1998) 271–280.

[34] V. Subramanian, E. Wolf, P. Kamat, Semiconductor-metal composite nanostructures. To what extent metal nanoparticles (Au, Pt, Ir) improve the photocatalytic activity of TiO_2 films, Journal of Physical Chemistry B 105 (2001) 11439–11446.

[35] W.S. Kuo, P.H. Ho, Solar photocatalytic decolonization of methylene blue in water, Chemosphere 45 (2001) 77–83.

[36] Z. Liu, Q. Liu, Y. Huang, Y. Ma, S. Yin, X. Zhang, W. Sun, Y. Chen, Organic photovoltaic devices based on a novel acceptor material: graphene, Advanced Materials 20 (2008) 3924–3930.

[37] G.K. Ramesha, A.V. Kumara, H.B. Muralidhara, S. Sampath, Graphene and graphene oxide as effective adsorbents toward anionic and cationic dyes, Journal of Colloid and Interface Science 361 (2011) 270–277.

[38] R. Velmurugan, M. Swaminathan, An efficient nanostructured ZnO for dye sensitized degradation of reactive red 120 dye under solar light, Solar Energy Materials and Solar Cells 95 (2011) 942–950.

[39] V. Rupa, D. Manikandan, D. Divakar, T. Sivakumar, Effect of deposition of Ag on TiO_2 nanoparticles on the photodegradation of Reactive Yellow-17, Journal of Hazardous Materials 147 (2007) 906–913.

[40] M. Yamanaka, K. Hara, J. Kudo, Bactericidal actions of a silver ion solution on *Escherichia coli*, studied by energy-filtering transmission electron microscopy and proteomic analysis, Journal of Applied and Environmental Microbiology 71 (2005) 7589–7593.

[41] H.R. Pant, D.R. Pandeya, K.T. Nam, W. Baek, S.T. Hong, H.Y. Kim, Photocatalytic and antibacterial properties of a TiO_2/nylon-6 electrospun nanocomposite mat containing silver nanoparticles, Journal of Hazardous Materials 189 (2011) 465–471.